PAPER

Check for updates

Preparation and photocatalytic activity of ZnGa₂O₄-β-Ga₂O₃ thin films†

Premrudee Promdet, [ID] Claire J. Carmalt [ID] and Ivan P. Parkin [ID] *

$ZnGa_2O_4$ and $ZnGa_2O_4$-β-Ga_2O_3 thin films were prepared *via* aerosol-assisted chemical vapor deposition (AACVD) using various ratios of the Zn and Ga precursors, resulting in the formation of amorphous $ZnGa_2O_4$ and Ga_2O_3. The formation of crystalline zinc gallate and heterostructure zinc gallate thin films was achieved by annealing the resulting films at high temperatures under air. The $ZnGa_2O_4$-β-Ga_2O_3 thin films showed enhanced photocatalytic activity compared with $ZnGa_2O_4$. The photocatalytic enhancement of the $ZnGa_2O_4$-β-Ga_2O_3 is explained by the formation of type-II band alignment at the interfaces between $ZnGa_2O_4$ and Ga_2O_3, resulting in enhanced photoinduced charge separation in the material.

1. Introduction

Oxide semiconductors have attracted much interest as an effective material for photocatalysts because of their high photocatalytic activity and mechanical and chemical durability.[1–3] Semiconductor-based photocatalysts have been applied for various applications, such as for self-cleaning, organic/inorganic pollutant decomposition, photoelectrochemical water splitting and antimicrobial coatings. Since the first study on p-block metal oxides of MIn_2O_4, M_2SnO_4 and $M_2Sb_2O_7$ (M = Ca, Sr) was reported by Inoue *et al.*,[4–7] semiconductors with a d^{10} electronic configuration have been widely studied and show promise as photocatalysts.[8–12] Among the p-block metal oxide photocatalysts, zinc gallate ($ZnGa_2O_4$) is also a promising photocatalyst and has been applied to water splitting,[13–15] organic pollutant degradation[16] and CO_2 reduction[17,18] applications under UV irradiation. However, $ZnGa_2O_4$ has had limited practical success due to its wide band gap energy (4.1–4.5 eV) and high recombination rate of the electrons and holes,[19] resulting in low photocatalytic performance. Therefore, broadening the light absorption and preventing the rapid recombination of the photogenerated electron–hole pairs of $ZnGa_2O_4$ photocatalysts, has become an area of focus.

Doping $ZnGa_2O_4$ with foreign ions is one approach to broaden the light absorption and improve the photocatalytic performance. Doping $ZnGa_2O_4$ with cations has been investigated showing improved visible light absorption.[20,21] Although the band gap was successfully reduced, some metal-doped $ZnGa_2O_4$ showed low photocatalytic efficiency due to rapid electron–hole recombination.[22] The formation of heterojunction structures is an attractive strategy to improve the photocatalytic properties of $ZnGa_2O_4$ by increasing the charge separation in photocatalytic processes. Heterojunction structures, such as $ZnGa_2O_4$/N-rGO[14] and $ZnO/ZnGa_2O_4$,[23] have been developed for improving the photocatalytic performance of $ZnGa_2O_4$.

Many methods have been used to synthesize $ZnGa_2O_4$ particles or thin films including hydrothermal,[24] solid-state,[25] sol–gel,[26] chemical vapor deposition,[27] and RF magnetron sputtering.[28] Among the large number of synthesis methods to produce $ZnGa_2O_4$ materials, the synthesis of thin films is widely convenient for practical applications compared with powders, due to the problems in the separation and recovery of powders. Aerosol-assisted chemical vapor deposition (AACVD) is a promising technique for thin film preparation because it is a simple, scalable, and cost-efficient technique that allows good control over physical and chemical properties.[29,30] In AACVD, precursors with low vapor pressure are dissolved in an appropriate solvent and the solution is aerosolized and transported into the CVD chamber using a carrier gas. The chemical composition of the starting material can play a crucial role in influencing the chemical and physical properties of the deposited films.

In this study, the formation of crystalline zinc gallate and heterostructure zinc gallate ($ZnGa_2O_4$-β-Ga_2O_3) thin films was studied. A deeper understanding of the effect of the heterostructure formation on band alignment, charge transfer and photocatalytic activity is required to explain the phenomena at the interfaces between $ZnGa_2O_4$ and Ga_2O_3.

2. Experimental section

2.1. Preparation of ZnGa₂O₄ and ZnGa₂O₄-β-Ga₂O₃ thin films

Zinc acetylacetonate [$(Zn(C_5H_7O_2)_2)$], 99.9% and gallium acetylacetonate [$(Ga(C_5H_7O_2)_3$], 99.9%) from Sigma Aldrich were used

Materials Chemistry Centre, Department of Chemistry, University College London, 20 Gordon Street, London WC1H 0AJ, UK. E-mail: i.p.parkin@ucl.ac.uk

Paper

as the zinc and gallium source materials, respectively. In a round bottom flask, solutions for AACVD were prepared by dissolving 0.5 mmol of zinc acetylacetonate and different amounts of gallium acetylacetonate (0.5, 0.7 and 1.0 mmol) in 40 mL methanol. Using a piezoelectric ultrasonic humidifier, a precursor mist was created and delivered to the reaction chamber with a flow rate of 1.0 L min^{-1} nitrogen gas. The deposition was carried out in a reactor at 400 °C. The obtained films were then annealed at 700 °C in air for 5 h, yielding clear thin films.

2.2. Analytical methods

Film morphology and thickness were studied using top- and side-view scanning electron microscopy (SEM) in a JEOL6301 instrument (10 kV). X-ray diffraction (XRD) analysis was carried out using a Bruker-Axs D8 (GADDS) diffractometer. The instrument operated with a monochromated Cu X-ray source with Cu K$_{\alpha1}$ ($\lambda = 1.54056$ Å) and Cu K$_{\alpha2}$ radiation ($\lambda = 1.54439$ Å) emitted with an intensity ratio of 2 : 1 and a 2D area X-ray detector with a resolution of 0.01°. Films were analyzed with a glancing incident angle (θ) of 1°. The diffraction patterns obtained were confirmed using database standards. UV/Vis spectroscopy was performed using a double monochromated PerkinElmer Lambda 950 UV/Vis/NIR spectrophotometer in the 300–800 nm range. X-Ray photoelectron spectroscopy (XPS) was performed using a Thermo K alpha spectrometer with monochromated Al Kα radiation, a dual beam charge compensation system and constant pass energy of 50 eV. Survey scans were collected in the range of 0–1200 eV. High-resolution XPS spectra were used for the principal peaks of Zn (2p) and Ga (2p), and deconvoluted using CasaXPS software with the calibration of C1s at 284.5 eV. The surface roughness of the films was characterized by atomic force microscopy (AFM) on a Keysight 5600LS scanning probe microscope taken at a scale of 5 μm × 5 μm.

2.3. Photocatalytic tests

The intrinsic photocatalytic properties of the films were investigated through the photodegradation of octadecanoic (stearic acid), which was used here as a model organic pollutant.[31] Stearic acid is very stable under UV irradiation in the absence of a photocatalyst. In these experiments, the films were dip coated with a thin layer of stearic acid (0.05 M solution in chloroform) and then monitored under UVC irradiation over a period of 32 h using a PerkinElmer RX-I Fourier transform infrared (FTIR) spectrometer. Plots of integrated areas of characteristic C–H infrared bands at 2923 and 2853 cm^{-1} were produced and the photodegradation rates were estimated from linear regression of the initial 30–50% of the curves. A conversion factor from the literature (1 cm^{-1} = 9.7 × 10^{15} molecules of stearic acid)[32] allowed for the estimation of the number of molecules of stearic acid degraded upon irradiation time. The light source used was a UVC (λ = 254 nm) Vilber-Lourmat BLB lamp (2 × 8 W, I = 1.0 mW cm^{-2}). The irradiance of the lamp was measured using a UVX radiometer (UVP).

3. Results and discussion

Amorphous thin films were grown on quartz substrates using aerosol-assisted chemical vapor deposition (AACVD) at 400 °C, as detailed in the experimental section. On the heated substrates, the precursors react and deposit on the substrates. The unreacted precursors and waste products are carried away to the exhaust, as shown in Fig. S1 (ESI†). A series of zinc gallate thin films were deposited using different molar ratios of Zn/Ga in the precursor mixture, resulting in the Zn/Ga mole ratios of 0.45, 0.26 and 0.17 in the films, as determined by elemental analysis (EDS), henceforth referred to as **ZG**-[Zn/Ga mole ratio], namely **ZG**-0.45, **ZG**-0.26 and **ZG**-0.17, respectively. X-ray diffraction (XRD) of the as-deposited films from AACVD showed no patterns and therefore they were presumed to be amorphous (Fig. S2, ESI†).

The amorphous phase was analyzed by XPS, where the energy separation between the Zn 2p$_{3/2}$ and Ga 2p$_{3/2}$ peaks was studied. The energy separation between Zn 2p$_{3/2}$ and Ga 2p$_{3/2}$ peaks (ΔE) has been used as a tool to distinguish whether the obtained product is a complete ZnGa$_2$O$_4$ or a composite of ZnO and Ga$_2$O$_3$, where the formation of ZnGa$_2$O$_4$ provides lower ΔE compared with a mixture of ZnO and Ga$_2$O$_3$.[33,34] In this work, ΔE of a mixture of commercial ZnO and Ga$_2$O$_3$ was studied providing a value of 96.6 eV. It was found that ΔE of the
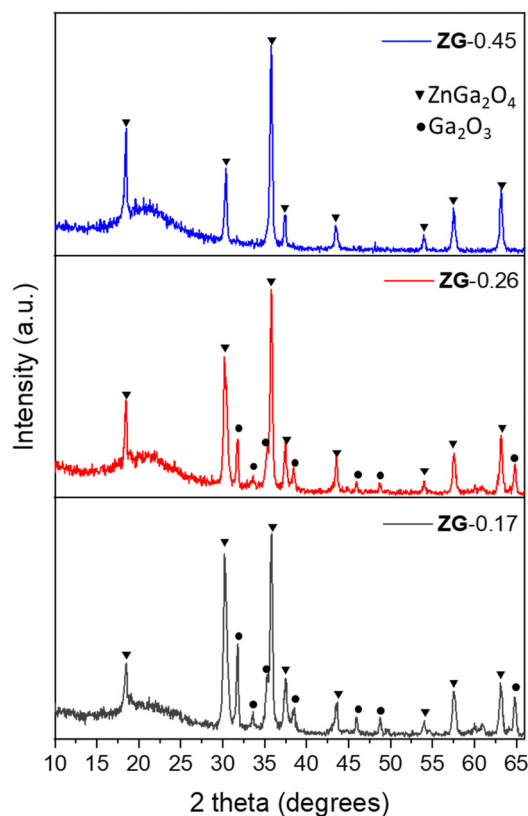

Fig. 1 XRD patterns of thin films annealed under air on quartz substrates at 700 °C of **ZG**-0.45, **ZG**-0.26 and **ZG**-0.17, respectively. Triangle symbols correspond to cubic-phase ZnGa$_2$O$_4$ (JCPDS no. 86-0415) and circle symbols correspond to β-Ga$_2$O$_3$ (JCPDS no. 43-1012).
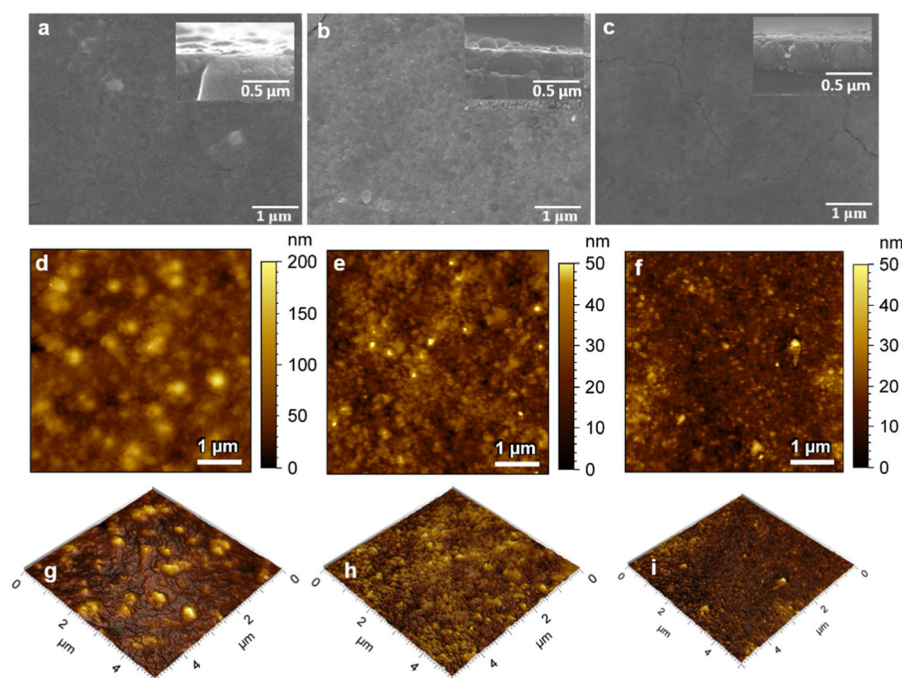
Fig. 2 Scanning electron microscopy (SEM) of (a) **ZG**-0.45, (b) **ZG**-0.26 and (c) **ZG**-0.17. Atomic Force Microscopy (AFM) images showing the surface morphology (top) and 3D images (bottom) of (d), (g) **ZG**-0.45, (e), (h) **ZG**-0.26 and (f), (i) **ZG**-0.17 thin films on quartz substrates prepared by the AACVD method at different mole ratios of Zn and Ga in the precursor mixture. The surface topography of the annealed films investigated by AFM, taken with a scale of 5 μm × 5 μm.

commercial mixture is higher than ΔE of the as-deposited amorphous thin films giving a value of 96.2 eV (Table S1, ESI†). This indicates the formation of zinc gallate under AACVD. The amorphous thin films were annealed under air at 700 °C, resulting in the formation of crystalline zinc gallate, which was confirmed by XRD as shown in Fig. 1. For those samples with low Ga content (**ZG**-0.45) only the pattern of cubic-phase $ZnGa_2O_4$ (JCPDS no. 86-0415)[35] was found. Relatively high Ga contents (**ZG**-0.26 and **ZG**-0.17), showed additional reflection peaks that were consistent with β-Ga_2O_3 (JCPDS no. 43-1012).[22,36]

The morphology and cross-section SEM images of the samples are shown in Fig. 2(a)–(c). SEM analysis showed similar surface morphologies in all thin films, with the thickness of **ZG**-0.45, **ZG**-0.26 and **ZG**-0.17 being 230, 280 and 340 nm, respectively. The surface topography of the annealed films (**ZG**-0.45, **ZG**-0.26 and **ZG**-0.17) was investigated by AFM, taken with a scale of 5 μm × 5 μm, as shown in Fig. 2.

Inspection of these images shows that the surface area and surface roughness of the thin films was not significantly affected by the ratio of Zn and Ga in the films. The surface roughness (rms roughness) of the annealed films (**ZG**-0.45, **ZG**-0.26 and **ZG**-0.17) was 63, 51 and 73, respectively, with surface areas of 26.7, 25.6 and 25.7 μm^2, respectively, as depicted in Table 1.

High-resolution XPS was further employed to investigate the composition and surface electron state of the thin films. Fig. 3 shows the XPS spectra revealing (a) Ga 2p and (b) Zn 2p of the films **ZG**-0.45, **ZG**-0.26 and **ZG**-0.17, respectively. Binding energy (BE) calibration was carried out using the C1s peak located at 284.5 eV. The XPS spectrum of the **ZG**-0.45 reveals a symmetric peak for the Ga 2p orbital, with a BE of 1118.5 eV, while the spectra of **ZG**-0.26 and **ZG**-0.17 can be deconvoluted into two peaks, with binding energy values of Ga $2p_{3/2}$ at 1118.4 and 1119.8 eV, respectively, which are associated with Ga^{3+} species in Ga_2O_3 and $ZnGa_2O_4$, respectively.[37]

Table 1 Structural, optical, and functional parameters of $ZnGa_2O_4$ and $ZnGa_2O_4$-β-Ga_2O_3 heterojunction films prepared with different ratios of zinc acetylacetonate and gallium acetylacetonate in the precursor mixture

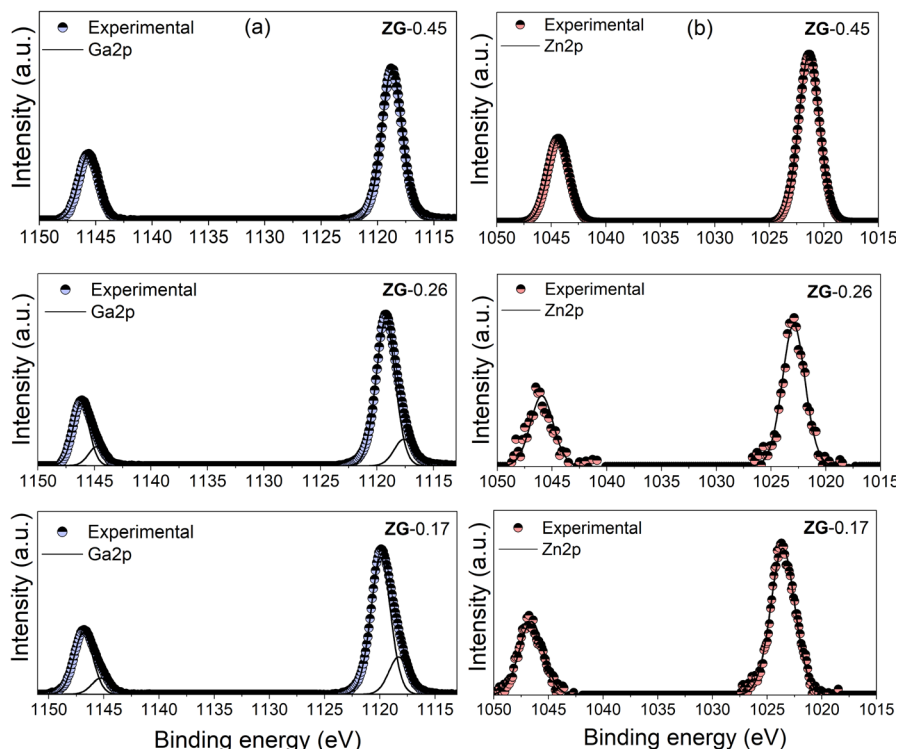| Sample	Zn/Ga atomic ratio		$ZnGa_2O_4$: Ga_2O_3	E_g (eV)	Film thickness (nm)	Surface area (μm^2)	RMS roughness (nm)	Surface area (μm^2)	$\xi \times 10^{-4}$ (molecules photon^{-1})
	In precursor solution	In as-deposited thin films							
ZG-0.45	1.0	0.45	9 : 1	5.2	230	26.69	63	26.69	0.50
ZG-0.26	0.7	0.26	1 : 1	5.1	280	25.59	51	25.59	1.64
ZG-0.17	0.5	0.17	1 : 2	4.9	340	25.67	74	25.67	0.80

Fig. 3 High-resolution XPS of (a) Ga 2p and (b) Zn 2p spectra of **ZG**-0.45, **ZG**-0.26 and **ZG**-0.17 deposited by AACVD on quartz.

The XPS spectrum of the Zn $2p_{1/2}$ peaks in the films was ~1022 eV, which could be related to the formation of $ZnGa_2O_4$.[38] To investigate the vertical distribution of $ZnGa_2O_4$ and Ga_2O_3 in the films, the Zn/Ga ratio was calculated using XPS depth profiling shown in Fig. S3 (ESI†). The Zn/Ga atomic ratio of thin films with etching shows that there is a homogenous mix of $ZnGa_2O_4$ and Ga_2O_3 in the thin films (**ZG**-0.45, **ZG**-0.26 and **ZG**-0.17).

The light absorption properties of the materials were studied by using UV-vis spectroscopy. The absorption edges of **ZG**-0.45, **ZG**-0.26 and **ZG**-0.17 were located at around 250 nm. The band gap energy of the materials was determined from the Tauc plot for indirect band gap absorption, as shown in Fig. 4(a). The samples (**ZG**-0.45, **ZG**-0.26 and **ZG**-0.17) had E_g values of 5.2, 5.1 and 4.9 eV, respectively.

The photocatalytic activity of the thin films was evaluated by testing the degradation rate of stearic acid, a model organic pollutant under UVC irradiation (BLB lamp, 1.0 mW cm^{-1}), as shown in Fig. 5 and Table 1. In the absence of catalyst, the detected concentration of stearic acid was stable under illumination, while the presence of catalyst (**ZG**-0.45, **ZG**-0.26 and **ZG**-0.17) leads to obvious degradation of stearic acid. The degradation of steric acid under irradiation results from the redox reactions of steric acid by photogenerated electrons and holes on the photocatalytic surface, providing the production of non-toxic CO_2 and H_2O.[39,40] The corresponding degradation curves are plotted against irradiation time in Fig. 5(a). The trend of degradation curves was as expected with the $ZnGa_2O_4$-β-Ga_2O_3 heterostructure thin film (**ZG**-0.26 and **ZG**-0.17) being a
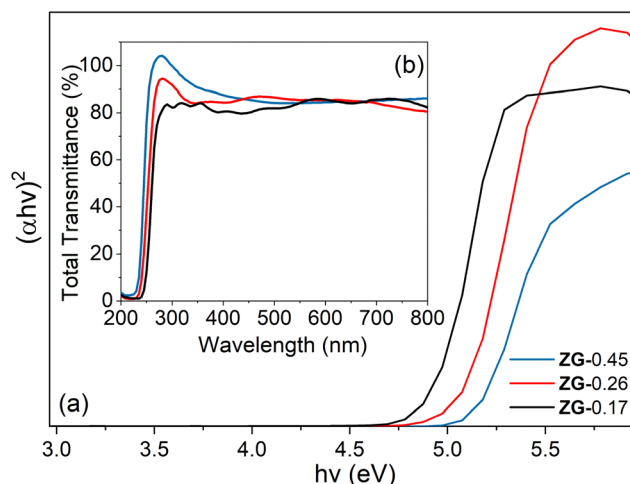

Fig. 4 (a) Tauc plot allowing an estimation of the band gap energies and the inset figure (b) shows the UV-Vis total transmittance of the annealed samples (**ZG**-0.45, **ZG**-0.26 and **ZG**-0.17) deposited by the AACVD method at different mole ratios between Zn/Ga in the precursor mixture of 1, 0.7 and 0.5, respectively.

more effective photocatalyst than $ZnGa_2O_4$ (**ZG**-0.45). In the case of **ZG**-0.26, with the ratio between $ZnGa_2O_4$ and Ga_2O_3 being 1 : 1, this provided higher photocatalytic performance, compared with the other thin films. As mentioned above, the surface area of the thin films was similar, and the photocatalytic efficiency was independent of the thickness of the thin films (Table 1). The apparent enhancement could then be

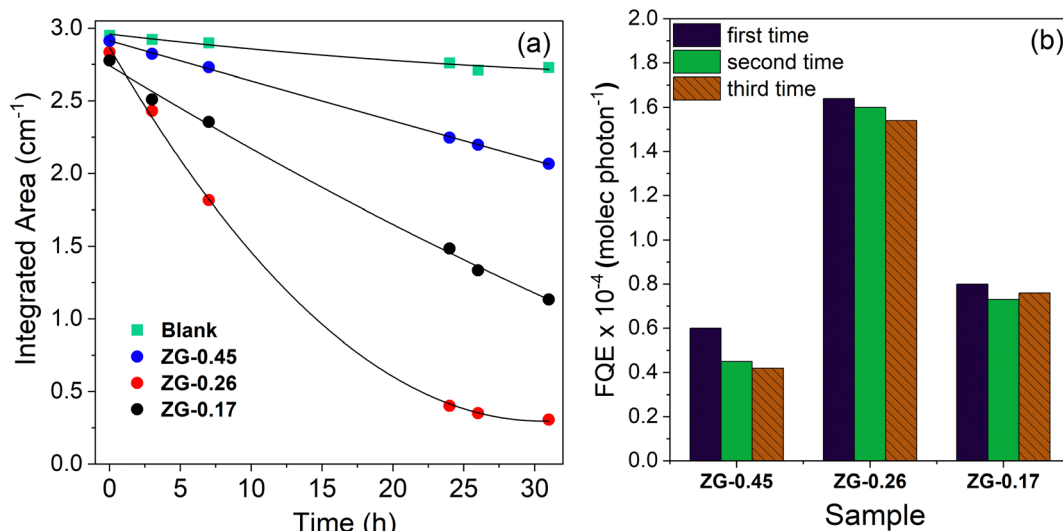inging

ing

ing

Fig. 5 (a) Integrated area of the IR spectra obtained from the initial rates of photodegradation of stearic acid upon irradiation time under UV illumination (UVC, λ = 254 nm, I = 1.0 mW cm^{-2}), with thin films (**ZG**-0.45, **ZG**-0.26 and **ZG**-0.17) acting as photocatalysts in the photodegradation. (b) Corresponding formal quantum efficiencies (ξ), given as molecules degraded per incident photon (units, molecules photon^{-1}), upon cycling experiments. A blank reference corresponds to the quartz substrate without the photocatalytic coating.
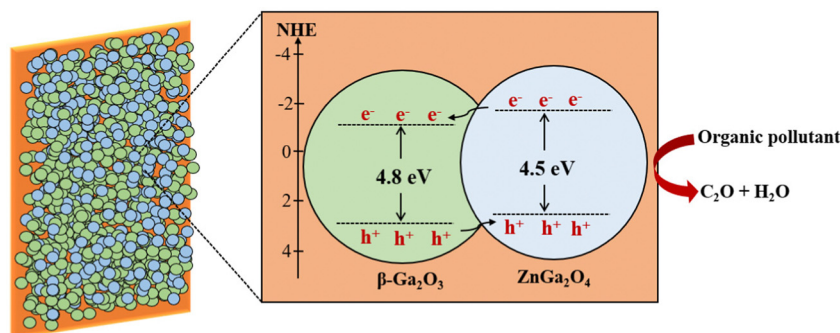
Scheme 1 A schematic description of charge transfers across the ZnGa$_2$O$_4$-β-Ga$_2$O$_3$ heterojunction.

related to the optimal ratio between ZnGa$_2$O$_4$ and Ga$_2$O$_3$ in the thin film.

The fitting of the initial degradation steps (zero-order kinetics) allowed for the estimation of the formal quantum efficiencies (ξ, units molecules photon^{-1}), given as the number of acid molecules degraded per incident photon (Fig. 5(b)). The cycle experiments resulted in a slight drop of the initial ξ values of the thin films. The drop of photocatalytic performance in the cycling experiments might be due to carbon contamination during the photodegradation of organic pollutants.

The higher photocatalytic performance of heterostructures (**ZG**-0.26 and **ZG**-0.17) might result from the formation of a heterojunction, which is an interface between the two regions of dissimilar semiconductors. In order to classify the type of band alignment in the interface, the valence band potential and band gap energy of ZnGa$_2$O$_4$ and β-Ga$_2$O$_3$ were considered. The band structures of ZnGa$_2$O$_4$ and β-Ga$_2$O$_3$ were analyzed using XPS showing that the valence band potential of β-Ga$_2$O$_3$ was 1.5 eV more positive than that of ZnGa$_2$O$_4$.[22] ZnGa$_2$O$_4$ has a wide bandgap energy of $\sim$4.1–4.5 eV being similar to the

bandgap energy of β-Ga$_2$O$_3$ (4.8 eV). Therefore, the band alignment of the ZnGa$_2$O$_4$-β-Ga$_2$O$_3$ heterojunction could be a type-II band alignment, which can enhance charge separation, as shown in Scheme 1.

The photogenerated electrons tend to migrate from the conduction band (CB) of ZnGa$_2$O$_4$ to that of β-Ga$_2$O$_3$, while the generated holes transfer from β-Ga$_2$O$_3$ to ZnGa$_2$O$_4$. Consequently, the recombination process in this material is decreased, benefiting the enhancement of the photocatalytic performance. The higher photocatalytic performance of **ZG**-0.26 than **ZG**-0.17 might result from achieving an ideal ratio between ZnGa$_2$O$_4$ and β-Ga$_2$O$_3$ (1:1) in the ZnGa$_2$O$_4$-β-Ga$_2$O$_3$ heterojunction, resulting in the increase of the heterojunction interface in the material.

4. Conclusion

In this research, the ability to tune the composition of ZnGa$_2$O$_4$ and β-Ga$_2$O$_3$ thin films by varying the ratios of Zn and Ga

precursors in the starting mixture under aerosol-assisted chemical vapor deposition (AACVD) has been demonstrated. The optimal ratio between the Zn and Ga precursor was found to be 0.7, which showed promising photocatalytic performance of the final product (**ZG**-0.26). The ZnGa$_2$O$_4$-β-Ga$_2$O$_3$ heterojunction possesses type-II band alignment, resulting in enhanced photocatalytic properties of the material. This result is a step forward toward the fabrication of an optimized photocatalytic material and calls for the implementation of synthesis strategies of zinc gallate.

Conflicts of interest

There are no conflicts to declare.

Acknowledgements

References

1 J. J. Rueda-Marquez, I. Levchuk, P. Fernández Ibañez and M. Sillanpää, A Critical Review on Application of Photocatalysis for Toxicity Reduction of Real Wastewaters, *J. Cleaner Prod.*, 2020, **258**, DOI: **10.1016/j.jclepro.2020.120694**.

2 S. Dong, J. Feng, M. Fan, Y. Pi, L. Hu, X. Han, M. Liu, J. Sun and J. Sun, Recent Developments in Heterogeneous Photocatalytic Water Treatment Using Visible Light-Responsive Photocatalysts: A Review, *RSC Adv.*, 2015, **5**(19), 14610–14630, DOI: **10.1039/c4ra13734e**.

3 S. Banerjee, D. D. Dionysiou and S. C. Pillai, Self-Cleaning Applications of TiO$_2$ by Photo-Induced Hydrophilicity and Photocatalysis, *Appl. Catal., B*, 2015, **176–177**, 396–428, DOI: **10.1016/j.apcatb.2015.03.058**.

4 K. Ikarashi, J. Sato, H. Kobayashi, N. Saito, H. Nishiyama and Y. Inoue, Photocatalysis for Water Decomposition by RuO$_2$-Dispersed ZnGa$_2$O$_4$ with d^{10} Configuration, *J. Phys. Chem. B*, 2002, **106**(35), 9048–9053, DOI: **10.1021/jp020539e**.

5 J. Sato, N. Saito, H. Nishiyama and Y. Inoue, New Photocatalyst Group for Water Decomposition of RuO$_2$-Loaded p-Block Metal (In, Sn, and Sb) Oxides with d^{10} Configuration, *J. Phys. Chem. B*, 2001, **105**(26), 6061–6063, DOI: **10.1021/jp010794j**.

6 J. Sato, N. Saito, H. Nishiyama and Y. Inoue, Photocatalytic Activity for Water Decomposition of RuO$_2$-Loaded SrIn$_2$O$_4$ with d^{10} Configuration, *Chem. Lett.*, 2001, 868–869, DOI: **10.1246/cl.2001.868**.

7 J. Sato, N. Saito, H. Nishiyama and Y. Inoue, Photocatalytic Water Decomposition by RuO2-Loaded Antimonates, M$_2$Sb$_2$O$_7$ (M = Ca, Sr), CaSb$_2$O$_6$ and NaSbO$_3$, with d^{10} Cofiguration, *J. Photochem. Photobiol., A*, 2002, **148**(1–3), 85–89, DOI: **10.1016/S1010-6030(02)00076-X**.

8 K. Maeda and K. Domen, Solid Solution of GaN and ZnO as a Stable Photocatalyst for Overall Water Splitting under Visible Light, *Chem. Mater.*, 2010, **22**(3), 612–623, DOI: **10.1021/cm901917a**.

9 K. R. Reyes-Gil, E. A. Reyes-García and D. Raftery, Nitrogen-Doped In$_2$O$_3$ Thin Film Electrodes for Photocatalytic Water Splitting, *J. Phys. Chem. C*, 2007, **111**(39), 14579–14588, DOI: **10.1021/jp072831y**.

10 Q. Liu, Y. Zhou, J. Kou, X. Chen, Z. Tian, J. Gao, S. Yan and Z. Zou, High-Yield Synthesis of Ultralong and Ultrathin Zn$_2$GeO$_4$ Nanoribbons toward Improved Photocatalytic Reduction of CO$_2$ into Renewable Hydrocarbon Fuel, *J. Am. Chem. Soc.*, 2010, **132**(41), 14385–14387, DOI: **10.1021/ja1068596**.

11 Y. Hou, X. Wang, L. Wu, Z. Ding and X. Fu, Efficient Decomposition of Benzene over a β-Ga$_2$O$_3$ Photocatalyst under Ambient Conditions, *Environ. Sci. Technol.*, 2006, **40**(18), 5799–5803, DOI: **10.1021/es061004s**.

12 K. Maeda, T. Takata, M. Hara, N. Saito, Y. Inoue, H. Kobayashi and K. Domen, GaN: ZnO Solid Solution as a Photocatalyst for Visible-Light-Driven Overall Water Splitting, *J. Am. Chem. Soc.*, 2005, **127**, 8286–8287, DOI: **10.1021/ja0518777**.

13 M. Zhong, Y. Li, I. Yamada and J.-J. Delaunay, ZnO–ZnGa$_2$O$_4$ Core–Shell Nanowire Array for Stable Photoelectrochemical Water Splitting, *Nanoscale*, 2012, **4**(5), 1509–1514, DOI: **10.1039/C2NR11451H**.

14 X. P. Bai, X. Zhao and W. L. Fan, Preparation and Enhanced Photocatalytic Hydrogen-Evolution Activity of ZnGa$_2$O$_4$/N-RGO Heterostructures, *RSC Adv.*, 2017, **7**(84), 53145–53156, DOI: **10.1039/c7ra09981a**.

15 C. Zeng, T. Hu, N. Hou, S. Liu, W. Gao, R. Cong and T. Yang, Photocatalytic Pure Water Splitting Activities for ZnGa$_2$O$_4$ synthesized by Various Methods, *Mater. Res. Bull.*, 2015, **61**, 481–485, DOI: **10.1016/j.materresbull.2014.10.041**.

16 W. Zhang, J. Zhang, Z. Chen and T. Wang, Photocatalytic Degradation of Methylene Blue by ZnGa$_2$O$_4$ thin Films, *Catal. Commun.*, 2009, **10**(13), 1781–1785, DOI: **10.1016/j.catcom.2009.06.004**.

17 Q. Liu, D. Wu, Y. Zhou, H. Su, R. Wang, C. Zhang, S. Yan, M. Xiao and Z. Zou, Single-Crystalline, Ultrathin ZnGa$_2$O$_4$ Nanosheet Scaffolds to Promote Photocatalytic Activity in CO$_2$ Reduction into Methane, *ACS Appl. Mater. Interfaces*, 2014, **6**(4), 2356–2361, DOI: **10.1021/am404572g**.

18 Y. Zhang, P. Li, L. Q. Tang, Y. Q. Li, Y. Zhou, J. M. Liu and Z. G. Zou, Robust, Double-Shelled ZnGa$_2$O$_4$ hollow Spheres for Photocatalytic Reduction of CO$_2$ to Methane, *Dalton Trans.*, 2017, **46**(32), 10564–10568, DOI: **10.1039/c6dt04668a**.

19 P. Li, X. Zhao, H. Sun, L. Wang, B. Song, B. Gao and W. Fan, Theoretical Studies on the Form and Effect of N-Doping in an ZnGa$_2$O$_4$ Photocatalyst, *RSC Adv.*, 2016, **6**(78), 74483–74492, DOI: **10.1039/c6ra09655g**.

20 W. Zhang, J. Zhang, X. Lan, Z. Chen and T. Wang, Photo-catalytic Performance of ZnGa$_2$O$_4$ for Degradation of Methy-lene Blue and Its Improvement by Doping with Cd, *Catal. Commun.*, 2010, **11**(14), 1104–1108, DOI: **10.1016/j.catcom.2010.05.021**.

21 X. Xu, Y. Xie, S. Ni, A. K. Azad and T. Cao, Photocatalytic H$_2$ Production from Spinels ZnGa$_{2-x}$Cr$_x$O$_4$ ($0 \leq x \leq 2$) Solid Solutions, *J. Solid State Chem.*, 2015, **230**, 95–101, DOI: **10.1016/j.jssc.2015.05.029**.

22 X. Wang, S. Shen, S. Jin, J. Yang, M. Li, X. Wang, H. Han and C. Li, Effects of Zn^{2+} and Pb^{2+} Dopants on the Activity of Ga$_2$O$_3$-Based Photocatalysts for Water Splitting, *Phys. Chem. Chem. Phys.*, 2013, **15**(44), 19380–19386, DOI: **10.1039/c3cp53333f**.

23 M. Baojun, L. Keying, S. Weiguang and L. Wanyi, One-Pot Synthesis of ZnO/ZnGa$_2$O$_4$ Heterojunction with X/XY Struc-ture for Improved Photocatalytic Activity, *Appl. Surf. Sci.*, 2014, **317**, 682–687, DOI: **10.1016/j.apsusc.2014.08.089**.

24 M. Sun, D. Li, W. Zhang, Z. Chen, H. Huang, W. Li, Y. He and X. Fu, Rapid Microwave Hydrothermal Synthesis of ZnGa$_2$O$_4$ with High Photocatalytic Activity toward Aromatic Compounds in Air and Dyes in Liquid Water, *J. Solid State Chem.*, 2012, **190**, 135–142, DOI: **10.1016/j.jssc.2012.02.027**.

25 M. M. Can, G. Hassnain Jaffari, S. Aksoy, S. I. Shah and T. Firat, Synthesis and Characterization of ZnGa$_2$O$_4$ Parti-cles Prepared by Solid State Reaction, *J. Alloys Compd.*, 2013, **549**, 303–307, DOI: **10.1016/j.jallcom.2012.08.137**.

26 T. Sei, Y. Nomura and T. Tsuchiya, Preparation of ZnGa$_2$O$_4$ Thin Film by Sol–Gel Process and Effect of Reduction on Its Electric Conductivity, *J. Non-Cryst. Solids*, 1997, **218**, 135–138, DOI: **10.1016/S0022-3093(97)00163-4**.

27 C. E. Knapp, J. A. Manzi, A. Kafizas, I. P. Parkin and C. J. Carmalt, Aerosol-Assisted Chemical Vapour Deposition of Transparent Zinc Gallate Films, *ChemPlusChem*, 2014, **79**(7), 1024–1029, DOI: **10.1002/cplu.201402037**.

28 R. Reshmi, K. M. Krishna, R. Manoj and M. K. Jayaraj, Pulsed Laser Deposition of ZnGa$_2$O$_4$ Phosphor Films, *Surf. Coat. Technol.*, 2005, **198**(1–3 SPEC. ISS.), 345–349, DOI: **10.1016/j.surfcoat.2004.10.072**.

29 C. Sotelo-Vazquez, N. Noor, A. Kafizas, R. Quesada-Cabrera, D. O. Scanlon, A. Taylor, J. R. Durrant and I. P. Parkin, Multifunctional P-Doped TiO$_2$ Films: A New Approach to Self-Cleaning, Transparent Conducting Oxide Materials, *Chem. Mater.*, 2015, **27**(9), 3234–3242, DOI: **10.1021/cm504734a**.

30 A. M. Alotaibi, S. Sathasivam, B. A. D. Williamson, A. Kafizas, C. Sotelo-Vazquez, A. Taylor, D. O. Scanlon and I. P. Parkin, Chemical Vapor Deposition of Photocatalytically Active Pure Brookite TiO$_2$ Thin Films, *Chem. Mater.*, 2018, **30**(4), 1353–1361.

31 M. J. Powell, R. Quesada-Cabrera, W. L. Travis and I. P. Parkin, High-Throughput Synthesis of Core-Shell and Multi-Shelled Materials by Fluidised Bed Chemical Vapour Deposition. Case Study: Double-Shell Rutile-Anatase Parti-cles, *J. Mater. Chem. A*, 2015, **3**(33), 17241–17247, DOI: **10.1039/c5ta03526k**.

32 R. Quesada-Cabrera, C. Sotelo-Vazquez, J. C. Bear, J. A. Darr and I. P. Parkin, Photocatalytic Evidence of the Rutile-to-Anatase Electron Transfer in Titania, *Adv. Mater. Interfaces*, 2014, **1**(6), 1–7, DOI: **10.1002/admi.201400069**.

33 Y. Yuan, W. Du and X. Qian, ZnXGa$_2$O$_{3+x}$ ($0 \leq x \leq 1$) Solid Solution Nanocrystals: Tunable Composition and Optical Properties, *J. Mater. Chem.*, 2012, **22**(2), 653–659, DOI: **10.1039/c1jm13091a**.

34 L. Zou, X. Xiang, M. Wei, F. Li and D. G. Evans, Single-Crystalline ZnGa$_2$O$_4$ Spinel Phosphor via a Single-Source Inorganic Precursor Route, *Inorg. Chem.*, 2008, **47**(4), 1361–1369, DOI: **10.1021/ic7012528**.

35 T. A. Safeera, R. Khanal, J. E. Medvedeva, A. I. Martinez, G. Vinitha and E. I. Anila, Low Temperature Synthesis and Characterization of Zinc Gallate Quantum Dots for Opto-electronic Applications, *J. Alloys Compd.*, 2018, **740**(May), 567–573, DOI: **10.1016/j.jallcom.2018.01.035**.

36 J. Zhang, Z. Liu, C. Lin and J. Lin, A Simple Method to Synthesize β-Ga$_2$O$_3$ Nanorods and Their Photolumines-cence Properties, *J. Cryst. Growth*, 2005, **280**(1–2), 99–106, DOI: **10.1016/j.jcrysgro.2005.02.060**.

37 Y. B. Seung, W. S. Hee, W. N. Chan and J. Park, Synthesis of Blue-Light-Emitting ZnGa$_2$O$_4$ Nanowires Using Chemical Vapor Deposition, *Chem. Commun.*, 2004, (16), 1834–1835, DOI: **10.1039/b405592f**.

38 E. Chikoidze, C. Sartel, I. Madaci, H. Mohamed, C. Vilar, B. Ballesteros, F. Belarre, E. del Corro, P. Vales-Castro and G. Sauthier, *et al.*, P-Type Ultrawide-Band-Gap Spinel ZnGa$_2$O$_4$: New Perspectives for Energy Electronics, *Cryst. Growth Des.*, 2020, **20**(4), 2535–2546, DOI: **10.1021/acs.cgd.9b01669**.

39 J. Krýsa, G. Waldner, H. Měšťánková, J. Jirkovský and G. Grabner, Photocatalytic Degradation of Model Organic Pollutants on an Immobilized Particulate TiO$_2$ Layer. Roles of Adsorption Processes and Mechanistic Complexity, *Appl. Catal., B*, 2006, **64**(3–4), 290–301, DOI: **10.1016/j.apcatb.2005.11.007**.

40 M. I. Litter, Heterogeneous Photocatalysis: Transition Metal Ions in Photocatalytic Systems, *Appl. Catal., B*, 1999, **23**(2–3), 89–114, DOI: **10.1016/S0926-3373(99)00069-7**.